Influence of Heterogeneous Soils and Clutter on the Performance of Ground-Penetrating Radar for Landmine Detection

Kazunori Takahashi, *Member, IEEE*, Jan Igel, Holger Preetz, and Motoyuki Sato, *Fellow, IEEE*

***Abstract*—Ground-penetrating radar (GPR) has been studied for landmine detection and identification. Since this application employs higher frequencies as compared to conventional large-scale GPR measurements, the GPR performance is greatly influenced by soil properties and their spatial heterogeneity. In order to study the influence of soil heterogeneity on GPR performance, three types of soil were investigated. From the soil heterogeneity, GPR clutter was modeled with the aim of assessing the difficulty encountered in successful GPR performance. A handheld dual-sensor system that combines a metal detector and GPR was tested in these three test soils, and its performance for identifying buried objects was evaluated. The GPR performance obtained from the test showed a clear correlation with the modeled GPR clutter. Hence, the present study illustrates that clutter plays a major role in the detection of small objects in heterogeneous soil by GPR.**

***Index Terms*—Clutter, dielectric permittivity, geostatistics, ground-penetrating radar (GPR), landmine detection, scattering, soil heterogeneity.**

I. Introduction

GROUND-penetrating radar (GPR) has been studied extensively for landmine detection, as this technique is expected to improve the productivity of clearance operations by discriminating buried objects in a nondestructive manner, i.e., without excavation [1]. The identification of a buried object by GPR is based on its size and shape. There are various techniques proposed for discrimination based on other signatures of landmines. These include metal detector responses (e.g., [2]–[4]), nuclear quadrupole resonance (e.g., [5]–[7]), chemical vapor analysis/spectrometry (e.g., [8]), acoustic methods (e.g., [9]–[11]), and infrared detection (e.g., [12] and [13]). None of the aforementioned technologies except GPR has been fielded for humanitarian demining until now because of the complexity, high cost, and large size of these systems.

Manuscript received May 20, 2013; revised June 25, 2013; accepted July 1, 2013. Date of publication July 31, 2013; date of current version March 3, 2014. This work was supported in part by the Japan Society for the Promotion of Science under Grant-in-Aid for Scientific Research (C) 24612001 and the Federal Office of Defense Technology and Procurement, Germany.

K. Takahashi and M. Sato are with the Center for Northeast Asian Studies, Tohoku University, Sendai 980-8576, Japan (e-mail: kazunori.takahashi@cneas.tohoku.ac.jp; sato@cneas.tohoku.ac.jp).

J. Igel is with the Leibniz Institute for Applied Geophysics, 30655 Hannover, Germany (e-mail: jan.igel@liag-hannover.de).

H. Preetz is with the Construction Department of Lower Saxony, Federal Competence Center for Soil and Groundwater Protection/UXO Clearance, 30169 Hannover, Germany (e-mail: holger.preetz@ofd-bl.niedersachsen.de).

Color versions of one or more of the figures in this paper are available online at http://ieeexplore.ieee.org.

Digital Object Identifier 10.1109/TGRS.2013.2273082

GPR has been considered as the most promising subsurface sensing technique for landmine clearance operations in combination with a metal detector. This is because of its ability to detect both metallic and nonmetallic landmines as well as its imaging capability, simplicity, and relatively low production cost [14], [15]. Furthermore, the capability for imaging and postprocessing of data enables the identification of detected objects (e.g., [16]–[18]). A system combining GPR and a metal detector is commonly called a dual sensor. The system uses the metal detector as the primary sensor for the detection and localization of metal-containing objects, after which it switches to GPR as the secondary sensor for target identification.

GPR for landmine detection commonly employs relatively high frequencies [18]–[21] in order to detect and/or image small objects near the surface and also to reduce the size of the antennas (i.e., the size of the detectors) for easier handling and higher mobility. With high frequencies, GPR becomes more sensitive to the heterogeneity of the media surrounding the object, which results in unwanted scattering in the data. The unwanted scattered waves are commonly referred to as *clutter*. Clutter degrades the quality of the GPR data and makes their analysis and interpretation difficult. In the case of landmine detection, a false analysis or interpretation of the data may lead to an accidental detonation. The performance assessment of GPR is crucial and necessary in order to ensure the safety of clearance operations with GPR. Since clutter strongly influences performance, such an assessment must take into account soil heterogeneity and must be carried out at each site with a different type of soil and after drastic change of soil conditions prior to actual operations. This may require rapid measurements and analysis of soils. This analysis also allows us to assess the effectiveness of the technique, and thus, it may help in the selection of a suitable detection technique and in saving time and costs. Such a quick assessment method exists for metal detectors used in humanitarian demining that involves magnetic susceptibility measurements at one or two frequencies [22]. However, thus far, there has been no systematic assessment method established for GPR. Therefore, opinions from experts that are often based only on their impressions and experiences have always been used to foresee the effectiveness of using GPR.

We developed a simple method for modeling GPR clutter that calculates a typical value of clutter power from the heterogeneity of the soil. The method was demonstrated for one soil type with different heterogeneities during a short-term infiltration experiment [23], [24], which also included natural seasonal changes [25]. The model takes into account

heterogeneity in the dielectric permittivity of the soil. There are other properties that influence the propagation of electromagnetic waves such as electrical conductivity and magnetic permeability. However, in the normal ranges, their influence on reflectivity, which is the main cause of clutter, is usually very small as compared to that of dielectric permittivity [21], [26]. Therefore, heterogeneities in conductivity and permeability are often negligible.

In this paper, the modeling method is applied to three different soil types on which a GPR system developed specifically for landmine detection was tested. The modeled GPR clutter showed a correlation with the performance of the GPR system, which was evaluated by a blind test. The present paper illustrates the correlation and demonstrates the influence of heterogeneous soil on the performance of GPR for landmine detection and for other high-frequency GPR applications.

II. GPR Clutter Modeling

A. Characterization of Soil Heterogeneity

The modeling technique requires input parameters that characterize soil heterogeneity, so these parameters first need to be obtained. Perhaps, the most common way to measure dielectric permittivity of soil in the field is time domain reflectometry (TDR), and the spatial distribution can be obtained by carrying out TDR measurements at multiple locations on the ground surface. TDR gives the permittivity of the soil around the probes or the water content associated with permittivity by empirical (e.g., [27]) or mixing models (e.g., [28]), and thus, the measurement scale depends on the probe configuration. If relatively small probes (in our case 10 cm in length with 2-cm separation between the rods) are employed, the footprint may be similar to that of high-frequency GPR at a shallow depth. Furthermore, TDR typically uses frequencies ranging from 500 MHz to 1 GHz [21], which is comparable to the frequencies used for landmine detection and for relatively high-frequency GPR. Therefore, TDR measurements can be used to measure and characterize soil heterogeneity at a similar spatial scale and frequency range to that of high-frequency GPR for a shallow depth.

A semivariogram is a geostatistical analysis tool that can be used to quantify heterogeneity. For soil permittivity data measured on a 1-D profile $\varepsilon(x)$, the experimental semivariogram $\gamma(h)$ is calculated as follows [29]:

$$\gamma(h) = \frac{1}{2N_h} \sum_{i=1}^{N_h} [\varepsilon(x_i + h) - \varepsilon(x_i)]^2 \tag{1}$$

where h is the lag distance between two data points $\varepsilon(x_i + h)$ and $\varepsilon(x_i)$, and N_h is the number of data pairs with a constant lag distance h from all data points. Often, the semivariance $\gamma(h)$ increases with the lag distance h up to a certain value, after which it becomes constant. For lag distance h, the semivariance $\gamma(h)$ that becomes constant is referred to as the sill C; the corresponding h is called the range a. The range denotes the mean distance at which a data pair no longer correlates, and thus, it is equivalent to the correlation length or characteristic length [30]. The sill corresponds to the maximum variance within a data set and is thus an indication of the variability. An exponential semivariogram model with no nugget effect, given as [29]

$$\hat{\gamma}(h) = C\left[1 - \exp\left(\frac{-3h}{a}\right)\right] \tag{2}$$

is fitted to the experimental semivariograms in order to determine the range a and sill C of the spatial distribution in the field. Since the exponential model reaches its sill asymptotically, the practical range a is defined as the distance where the modeled semivariance reaches 95% of the sill [31], [32]. The semivariogram model is employed in this study because the exponential semivariogram is expected due to the distribution of distances between soil boundaries, which is the principal source of the variation [33]. Nevertheless, the semivariogram analysis is only to determine parameters a and C, which are required in the following section to build a dielectric sphere model for the calculation of clutter power, and the shape of a semivariogram model is not relevant for the calculation.

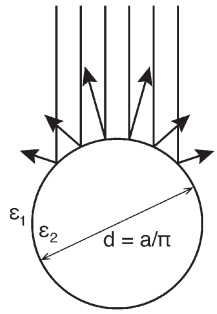

Fig. 1. Schematic illustration of the model for the calculation of backscattering power. The dielectric sphere model has a diameter d and permittivity ε_2, and it is embedded in a homogeneous dielectric space with a permittivity ε_1 [24].

B. Dielectric Sphere Model for GPR Clutter Power Calculation

A simple model is constructed with the model parameters obtained by the semivariogram, i.e., the correlation length a and variability C, as well as with the mean of the measured soil permittivity $\bar{\varepsilon}$. The model considered in this study is illustrated conceptually in Fig. 1. It consists of a dielectric sphere embedded in a homogeneous dielectric space. The homogeneous background is defined as having a dielectric permittivity equal to the mean permittivity, i.e., $\varepsilon_1 = \bar{\varepsilon}$. The circumference of the dielectric sphere is chosen to be equal to the correlation length, and thus, the diameter of the sphere d is defined as $d = a/\pi$, where a is the correlation length of the soil permittivity distribution determined by the geostatistical analysis described in the previous section. The permittivity of the sphere ε_2 is set so that the contrast with the ambient medium is equal to the square root of the variance as follows:

$$\Delta\varepsilon = \varepsilon_2 - \varepsilon_1 = \sqrt{2C}. \tag{3}$$

With this model, the radar cross section (RCS) that is proportional to the backscattering power of the dielectric sphere is calculated theoretically, assuming a monostatic configuration

and plane wave incidence. There are two ways to calculate the RCS for the model: the Mie solution and Rayleigh approximation. The Mie solution is the exact solution of Maxwell's equations and describes scattering by an arbitrarily sized particle [34]. Therefore, it is valid over all frequency and sphere size ranges including not only the Mie scattering region but also the Rayleigh scattering and optical regions. In contrast, the Rayleigh approximation describes scattering by a particle with a small size compared to a wavelength [35], and it is generally valid only in the Rayleigh scattering region. The Rayleigh approximation simplifies the Mie solution; however, it is not valid in the Mie scattering and optical regions. Our previous study illustrated that the clutter caused by heterogeneous topsoil and observed with a relatively high-frequency GPR can be characterized as Mie scattering [23]–[25]. Therefore, the Mie solution is employed in order to calculate the RCS of the dielectric sphere model for the clutter modeling.

According to the Mie solution, the RCS σ_s of a dielectric sphere is given as [35]

$$\sigma_s = \frac{1}{x^2}\left|\sum_n (2n+1)(-1)^n (a_n - b_n)\right|^2 \tag{4}$$

where $x = kr$, with k as the wavenumber in the ambient medium, and r is the radius of the sphere. In case there is no change in the magnetic permeability between the dielectric sphere and the ambient medium which is assumed in this study, the coefficients a_n and b_n are given by

$$a_n = \frac{m^2 j_n(mx)\left[x j_n(x)\right]' - j_n(x)\left[mx j_n(mx)\right]'}{m^2 j_n(mx)\left[x h_n^{(1)}(x)\right]' - h_n^{(1)}(x)\left[mx j_n(mx)\right]'} \tag{5}$$

$$b_n = \frac{j_n(mx)\left[x j_n(x)\right]' - j_n(x)\left[mx j_n(mx)\right]'}{j_n(mx)\left[x h_n^{(1)}(x)\right]' - h_n^{(1)}(x)\left[mx j_n(mx)\right]'} \tag{6}$$

where $m = \sqrt{\varepsilon_1/\varepsilon_2}$ denotes the refractive index. The functions $j_n(x)$ and $h_n^{(1)}(x)$ are the spherical Bessel function of first kind of order n and spherical Hankel function of order n, respectively. Primes indicate derivatives with respect to the argument. The summation in (4) is theoretically from $n = 1$ to ∞, but the infinite series can be truncated after $n_{max} = x + 4x^{1/3} + 2$ [35].

III. Characterization of Heterogeneous Test Soils

In order to test GPR systems for landmine clearance, three types of soils were prepared. Hereafter, they are called the following: "laterite," "magnetic sand," and "humus." These test soils are described as follows [26].

1) "Laterite" is an Fe-rich tropical weathered product whose parent rock was basalt. It is a red-colored clay loam with a low stone content (basalt) of approximately 2%–5%. Laterites are the most common tropical soil formation, and this test soil provided the same physical and chemical features of those in tropics.
2) "Magnetic sand" is an artificial mixture of calcareous sand and engineered magnetite in order to replicate soil with high magnetic susceptibility. The texture is coarse sand with a small amount of fine gravel (2%–5%).
3) "Humus" is a forest soil from the Bavarian Alps. The texture is loam with a high stone content (approximately 30%–40%) and high humus content.

TABLE I
Texture and Humus Content of Test Soils

	Laterite	Magnetic sand	Humus
Clay [% of mineral soil]	31.5	1.3	17.1
Silt [% of mineral soil]	39.4	7.0	40.7
Sand [% of mineral soil]	29.1	91.7	42.2
Humus [% of total soil]	0.8	<0.5	12.4

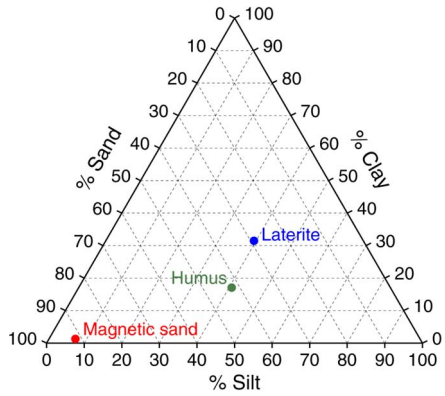

Fig. 2. Texture triangle of the test soils.

The texture and humus content of the test soils are provided in Table I, and a texture triangle is shown in Fig. 2.

The spatial distributions of dielectric permittivity in these soils were measured in the field at 10-cm intervals along 10-m profiles with a TDR (FOM/mts, Institute of Agrophysics of the Polish Academy of Science). The results are shown in Fig. 3, with the corresponding water content given by Topp's equation [27]. The TDR measurements as well as other geophysical measurements shown in the following were carried out a few days before the detector test, and there was no significant change or might only be limited changes in soil conditions in this period, which was verified by soil water content monitoring with permanently buried TDR probes [36]. It is very clear that magnetic sand showed very low mean permittivity and was much more homogeneous than the other soils. The different degree of heterogeneity of this soil is caused by a difference in texture and, thus, its affinity for holding water. In order to characterize the heterogeneity of the test soils, experimental semivariograms were calculated by (1) for the measured permittivity values. Fig. 4 shows the obtained semivariograms. The exponential model in (2) is fitted to the experimental semivariograms in order to determine the correlation length a and variability C. The statistical and geostatistical analyses of the spatial distributions of dielectric permittivity are summarized in Table II. The determined correlation length a and variability C are then put into the model for GPR clutter calculation as described in the previous section. Fig. 5 shows the modeled GPR clutter power for the three types of soil. The modeling

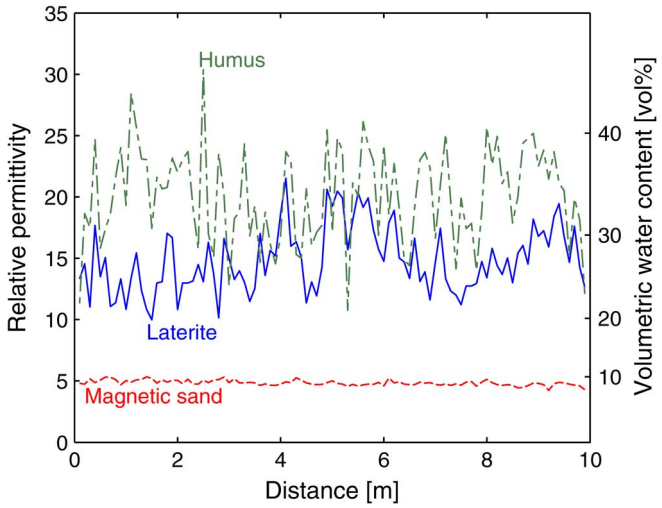

Fig. 3. Spatial distribution of relative dielectric permittivity of the test soils (laterite—solid line; magnetic sand—dashed line; humus—dash-dot line) measured by TDR at 10-cm intervals along a 10-m-long profile and corresponding water content given by Topp's equation.

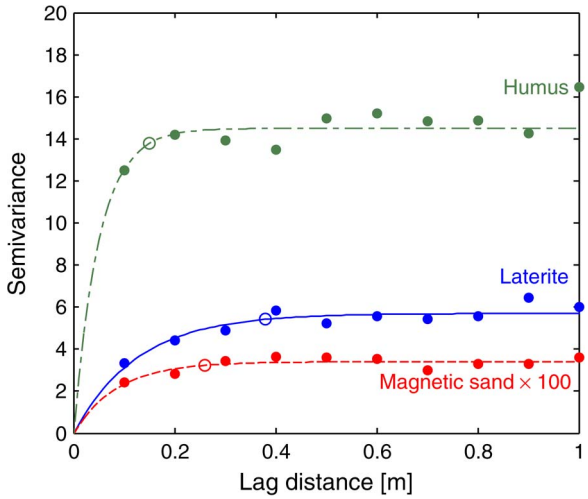

Fig. 4. Experimental semivariograms (dots) of relative permittivity measured by TDR and fitted exponential semivariogram models (laterite—solid line; magnetic sand—dashed line; humus—dash-dot line). Circles indicate effective correlation length and sill determined by the model fitting. Note that the semivariograms are not normal scored, and semivariance in magnetic sand is multiplied by a factor of 100 for better visibility.

TABLE II
SUMMARY OF THE DIELECTRIC PERMITTIVITY MEASUREMENTS AND ANALYSIS

	Laterite	Magnetic sand	Humus
Mean (relative permittivity)	14.9	4.8	20.1
Standard deviation	2.7	0.2	3.9
Coefficient of variation [%]	18.1	4.2	19.4
Correlation length [m]	0.38	0.26	0.15
Variability (sill)	5.7	0.03	14.5

was carried out at 0.8 GHz, which is the center frequency of the antennas used in the GPR system.

In addition to dielectric permittivity, electric conductivity and magnetic susceptibility of the test soils were also measured

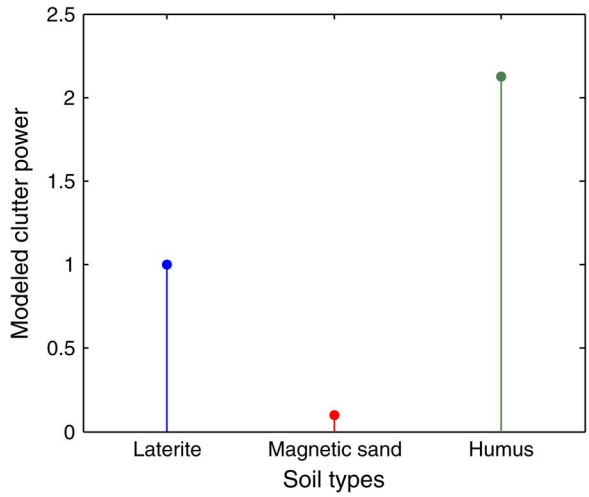

Fig. 5. Modeled clutter power for the three types of test soils.

in the field with a multichannel resistivity meter (Resecs, DMT) and susceptibility meter (MS2 and MS2D, Bartington), respectively, as well as in the laboratory on sampled soils by the spectral induced polarization (SIP) method (SIP Fuchs Lab, Radic Research) and with a susceptibility bridge (VFSM, Magnon). These properties are also known theoretically to be influential on electromagnetic fields. However, their influence on the reflectivity of electromagnetic signals is typically much less than the influence of dielectric permittivity [21], [26]. In the present study, clutter caused by soil heterogeneity is discussed. This is primarily related to reflections of electromagnetic waves from spatial variation in soil properties. If the influence of the variations of electrical conductivity and magnetic susceptibility on the reflectivity of electromagnetic waves is much smaller than that of dielectric permittivity, the influence of these properties can be neglected. Table III shows a summary of the measured electrical conductivity and magnetic susceptibility [26]. Both conductivity and susceptibility exhibited spatial variation. According to the coefficient of variation, the spatial variations of electrical conductivity in laterite and humus and of magnetic susceptibility in humus were significant compared to their mean. However, since all the soils showed very low mean conductivity and humus showed very low mean susceptibility, the influence of clutter due to the spatial variations of conductivity and susceptibility is irrelevant considering the much greater influence of dielectric permittivity. In order to assess the relevance of their influence in this study, reflection coefficients were roughly estimated from the variations of each property as shown in Fig. 6. The reflection coefficients were calculated with a simplified configuration assuming two media separated by a flat interface much larger than a wavelength and a normal incidence of plane waves as

$$\Gamma = \frac{Z_2 - Z_1}{Z_2 + Z_1} \tag{7}$$

where $Z = \sqrt{\mu/\varepsilon}$ denotes the intrinsic impedance of a medium. Magnetic susceptibility κ measured in the field is used to obtain magnetic permeability as $\mu = \mu_0(1 + \kappa)$, and complex permittivity ε is approximated and may be derived

TABLE III
SUMMARY OF THE ELECTRIC CONDUCTIVITY AND MAGNETIC SUSCEPTIBILITY MEASUREMENTS

	Laterite	Magnetic sand	Humus
Electric conductivity (*in situ*):			
Mean of static conductivity [mS/m]	2.45	0.32	7.68
Standard deviation	0.49	0.005	1.69
Coefficient of variation [%]	19.9	1.5	22.0
Correlation length [m]	n/a	n/a	0.34
Electric conductivity (lab):			
Conductivity at 1.5 Hz [mS/m]	3.22	0.20	9.96
Conductivity at 1.5 kHz [mS/m]	3.87	0.23	11.12
Magnetic susceptibility (*in situ*):			
Mean at 958 Hz [SIx10^{-5}]	2977	3324	18.5
Standard deviation	250	246	7.2
Coefficient of variation [%]	8.4	7.4	38.9
Correlation length [m]	0.41	0.34	0.45
Magnetic susceptibility (lab):			
Absolute frequency dependence in one decade (100 Hz vs. 1000 Hz) [SIx10^{-5}]	290	7	1.3
Relative frequency dependence [%]	6.0	0.1	1.2

The correlation lengths of electric conductivity in Laterite and Magnetic sand could not be determined.

from real-valued permittivity ε' and conductivity σ' measured in the field as [37]

$$\varepsilon = \varepsilon' - j\frac{\sigma'}{\omega}. \tag{8}$$

Medium 1 is set to have the mean of all the properties, and medium 2 is set so that the contrast to medium 1 in one property at a time is as much as the standard deviation s, i.e., for permittivity $\varepsilon_2 = \varepsilon_1 + \Delta\varepsilon = \bar{\varepsilon} + s$, while holding other properties constant at their mean. The figure shows that the reflection coefficients when setting the spatial variation of dielectric permittivity are much larger than those for other properties, typically more than two orders. Therefore, the variability of electrical conductivity and magnetic susceptibility has negligible influence on reflectivity compared to that of dielectric permittivity in these test soils, so they are not taken into account in the following discussions.

IV. TESTING DEMINING GPR SYSTEMS

A field test campaign for metal detectors and a dual sensor that employ GPR for landmine clearance operations took place in Germany in 2009 [38], [39] as a project of the International Test and Evaluation Program for Humanitarian Demining (ITEP). The test was carried out a few days after the permittivity measurements in the same soils. In 20-m test lanes with these soils, three mine-like targets, including

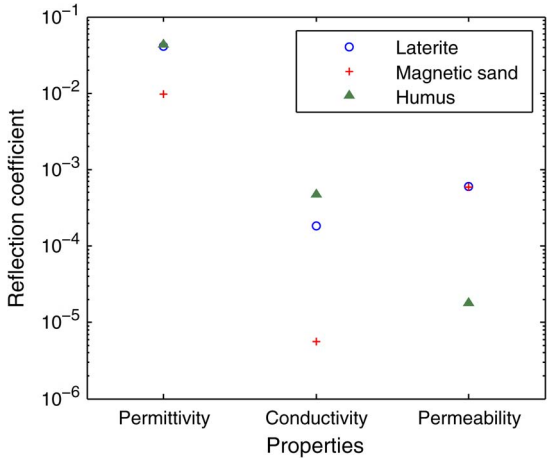

Fig. 6. Reflection coefficients in each soil due to the spatial variation of three soil properties calculated by assuming two media, a flat interface, and normal incidence of plane waves. The horizontal axis indicates properties of which the spatial variation is considered to obtain the reflection coefficient. For example, the values at "permittivity" show reflection coefficients when electromagnetic waves propagate from a medium with all properties at their mean to another medium with the permittivity difference as much as the standard deviation of the spatial variation while holding conductivity and permeability at their mean.

rendered-safe landmines, namely, a Gyata-64, a PPM-2, and a calibration target, were randomly planted. The calibration target imitates an antipersonnel landmine, and it consists of 10-cm-diameter plastic casing, a metal part, air gap, and wax, which has the same dielectric properties as explosives. In addition, various sizes of metal pieces, such as bullets, cartridges, and ammunition belts, were buried as metal clutter. These targets were buried a few months before the test in order to allow surrounding soils to settle. Their burial depths ranged from 2 to 15 cm. The locations of the test objects were unknown to the detector operators prior to the test runs, i.e., it was a blind test.

A dual-sensor system, which combined GPR and a metal detector, was tested in the campaign. In the operation of the dual-sensor system, the GPR function was used to identify objects that were detected and located by the metal detector. It is common to evaluate the performance of a metal detector by calculating the probability of detection (POD) and false alarm rate (FAR), which are the ratio of detected and buried mines and the number of false alarms per unit area, respectively. In order to evaluate the performance of the GPR function of dual-sensor systems in a similar manner, FAR reduction and POD loss are defined as [38], [39]

$$\text{FAR reduction} = 1 - \frac{\text{FAR by metal detector and GPR}}{\text{FAR by metal detector}} \tag{9}$$

$$\text{POD loss} = 1 - \frac{\text{POD by metal detector and GPR}}{\text{POD by metal detector}}. \tag{10}$$

FAR reduction indicates how many false alarms were rejected by using GPR, and it should be high for efficient clearance operations. POD loss is a measure to show how many landmines were wrongly identified as harmless metal pieces, and it should be low for safe operations. These measures are relative to the search result of the primary sensor (i.e., the metal detector) and are not directly influenced by the design of the experiment (i.e., the number of targets), although the associated estimation

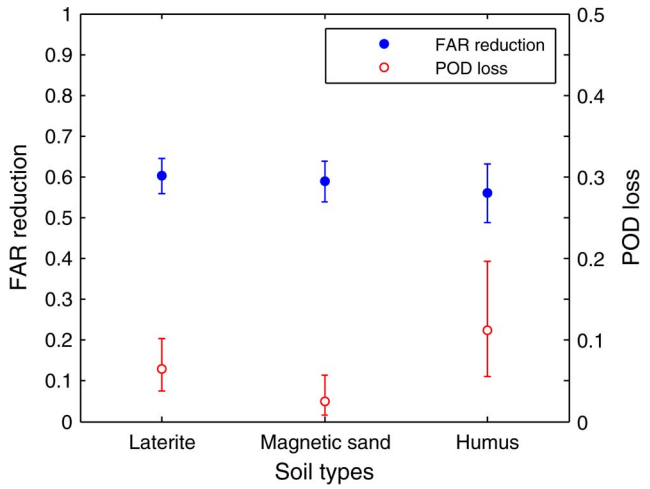

Fig. 7. GPR performance in FAR reduction (dots) and POD loss (circles) on the three types of test soil. The error bars show 95% confidence intervals.

accuracies (uncertainty) are affected. Ideally, FAR reduction is 1, which means that all the false alarms produced by a metal detector are rejected by GPR, and POD loss is 0, which means that no landmine detected by a metal detector is wrongly rejected by GPR. Even with the same dual-sensor system, the performance measures are expected to vary depending on the soil properties.

Fig. 7 shows the FAR reduction and POD loss obtained in the blind tests in the three test soils using a dual-sensor system. Their confidence intervals are provided to illustrate the accuracy of the estimations. They were calculated by assuming binominal distributions of both FAR reduction and POD loss. In the figure, FAR reduction is almost constant over different soil types, whereas POD loss varies from about 0.05 to 0.1 depending on soil types.

V. Clutter and Performance of GPR

In the previous sections, we obtained GPR performance in terms of FAR reduction and POD loss in the three test soils from a field test (Fig. 7). In addition, we calculated the expected GPR clutter for these soils, with TDR measurements in the field taking soil heterogeneity into account (Fig. 5).

To determine the level of difficulty of these test soils for GPR, we also carried out 1-D GPR scanning in reference lanes. Fig. 8 shows the obtained radar profiles with no signal processing applied. In the reference lanes, five rendered-safe landmines of PPM-2 with diameters of 13.4 cm were buried in straight lines in the three test soils at the positions of 0.6, 1.4, 2.2, 3.0, and 3.8 m and at depths of 25, 20, 15, 10, and 5 cm, respectively. A GPR (SIR-3000 with 1.5-GHz antennas, GSSI) was used to scan the locations immediately above the targets [Fig. 8(a), (c), and (e)] and 20 cm off the targets [Fig. 8(b), (d), and (f)]. The radar profile in magnetic sand with targets [Fig. 8(c)] exhibited very clear reflections from all landmines in a hyperbolic shape and did not have much clutter, which indicated that the soil was homogeneous. This is even more evident in Fig. 8(d), which shows less variation in signal amplitude in the lane where no target was buried. Reflections from all landmines can be observed in the profile in laterite [Fig. 8(a)]; however, the hyperbolic shapes were deformed due to the soil heterogeneity, and particularly for deeper mines, amplitudes were low due to the conductive and scattering attenuation of the soil. The profile in laterite without targets [Fig. 8(b)] exhibited more amplitude fluctuation than that in magnetic sand [Fig. 8(d)], which indicated that laterite is more heterogeneous, and thus, the data show more clutter and scattering loss. In the radar profile in humus [Fig. 8(e)], most of the reflections from landmines were difficult to recognize. Hyperbolic curves were not clear and were smeared. The reflections from landmines showed very low amplitude compared to those in other test soils, which was mainly the result of higher scattering loss due to soil heterogeneity. The profile without a target [Fig. 8(f)] exhibited more clutter with higher amplitude than other soils, which was comparable to the low-amplitude reflections from landmines. From these radar profiles, the modeled clutter power [Fig. 5] in test soils from only dielectric permittivity measurements looks reasonable. The adaptability of the model can be further confirmed by the comparison of the modeled clutter and clutter extracted from the radar profiles as shown in Fig. 9. Clutter was extracted from the radar profiles without targets [i.e., Fig. 8(b), (d), and (f)] by picking the highest amplitude values at each position, i.e., each radar trace, within a depth section of 15–25 cm, which is below the direct coupling. It is common knowledge that direct coupling disturbs and masks the hyperbolic signatures of shallow landmines (e.g., [14]). Direct coupling may be influenced by a rough ground surface, which may make the detection of hyperbolic signatures even more difficult. However, in this test, the ground surface was flattened because the scope of the study was the heterogeneity in soils. Note that the reflection from the deepest landmine was visible in magnetic sand even when measuring 20 cm off the targets [Fig. 8(d)]. This is due to the low scattering attenuation in this soil and wider radiation pattern in low-permittivity soil [40]. Thus, the obvious reflections of targets were excluded from the picking of the clutter. In Fig. 9, the picked clutter power at each position in the radar section was plotted with dots, and the modes and 95% confidence intervals are provided with circles and error bars, respectively, assuming that the clutter power was Rayleigh distributed. The modeled clutter (Fig. 5) and the extracted clutter (Fig. 9) agree very well; humus produced almost double the clutter power of laterite, and clutter in magnetic sand was much smaller than that for the other soils. Furthermore, the difficulty in recognizing landmines in radar profiles in Fig. 8 does not contradict the modeled clutter power and extracted clutter power.

In order to discuss further the influence of clutter in landmine detection and identification, GPR performance in terms of FAR reduction and POD loss defined in (9) and (10) was plotted as a function of clutter power in Fig. 10. As also shown in Fig. 7, FAR reduction is nearly constant around 0.6 considering the confidence intervals. However, it is clearly depicted that the POD loss increases linearly with clutter power. This demonstrates that GPR performance in terms of misidentification degrades as the power of GPR clutter caused by soil heterogeneity increases. This implies that the GPR performance in a particular type of soil can be assessed without actually testing detectors if the clutter power is known. GPR clutter is caused by soil heterogeneity mainly in dielectric permittivity; however, the relationship is not simple when relatively high frequencies are used. Therefore, clutter modeling is necessary to

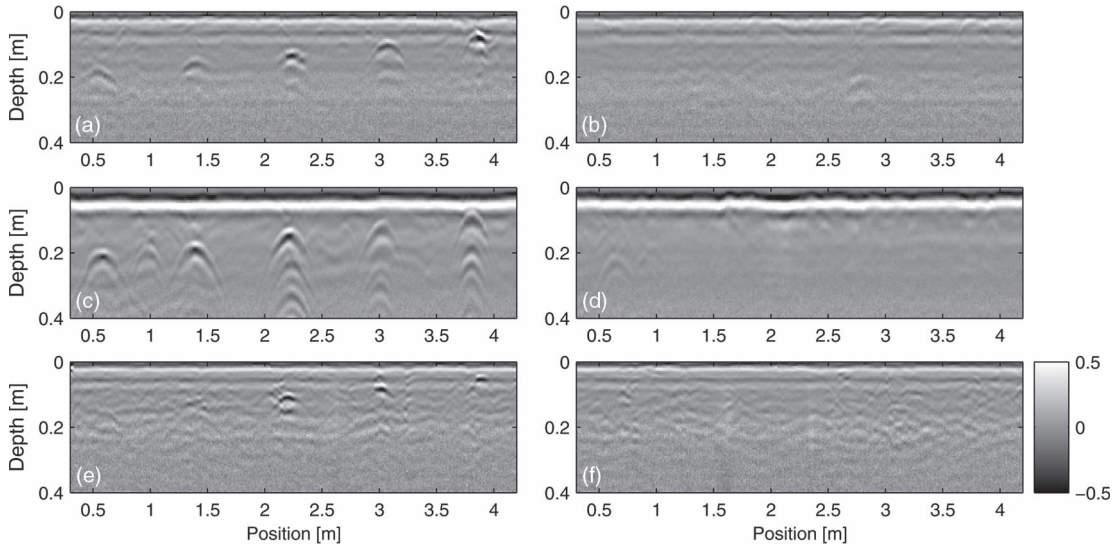

Fig. 8. GPR profiles acquired by GSSI SIR-3000 with 1.5-GHz antennas in (a) and (b) laterite, (c) and (d) magnetic sand, and (e) and (f) humus. The profiles at the left column are from scanning over the targets and at the right are from scanning 20 cm off the targets. Rendered-safe PPM-2 landmines were located at positions of 0.6, 1.4, 2.2, 3.0, and 3.8 m and at depths of 25, 20, 15, 10, and 5 cm, respectively. Time axes were converted to depth with mean permittivity of each soil (Table II).

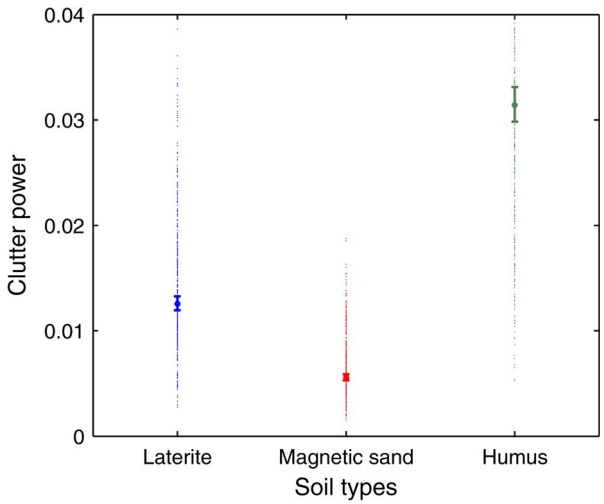

Fig. 9. GPR clutter power picked from measured data (Fig. 8). The circles indicate the mode, and the error bars show 95% confidence intervals.

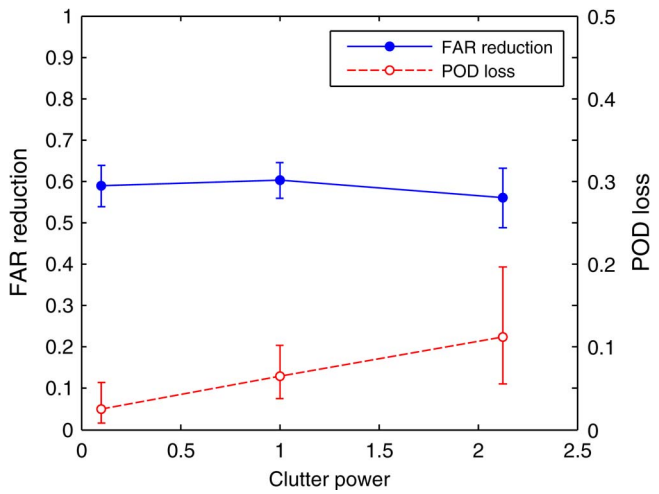

Fig. 10. GPR performance in FAR reduction (dots with solid line) and POD loss (circles with dashed line) as a function of modeled GPR clutter. The error bars show 95% confidence intervals.

predict GPR performance. The dielectric sphere model, which simplifies the scattering mechanism of electromagnetic waves in heterogeneous soil, showed practically reasonable results in this study.

VI. Discussions and Conclusion

It may be a common understanding that heterogeneous soils cause GPR clutter that degrades GPR performance. Therefore, GPR performance can be predicted by evaluating soil heterogeneity, which may typically be assessed by only first-order statistics such as variance and standard deviation. However, the present study showed that, in the case of GPR using relatively higher frequencies, both correlation length and variability have to be taken into account.

In this paper, three types of soil were evaluated. If only the coefficients of variation of dielectric permittivity are compared, magnetic sand would be very homogeneous, and laterite and humus would be almost equally heterogeneous (Table II). However, the clutter modeling shows that humus causes approximately twice as much clutter as laterite, i.e., humus is more heterogeneous for GPR. A similar discussion can be made for correlation length; it may be assumed that clutter is greater if the correlation length of permittivity variation is similar to the wavelength. Based on this assumption, the relative heterogeneity of soil may be defined as

$$H = 1 - \left| \frac{\lambda - a}{\lambda + a} \right| \tag{11}$$

where λ is the wavelength in the medium and a is the correlation length of permittivity variation. The scale takes values from 0 to 1, with larger values indicating more heterogeneous soil in terms of the spatial length of variation. The analysis in

this study was carried out at 0.8 GHz, which corresponds to wavelengths of 9.7, 17.0, and 8.4 cm at the mean permittivity of laterite, magnetic sand, and humus, respectively, and the respective H values for these soils were 0.4, 0.8, and 0.7. From these values alone, laterite would be the most homogeneous soil, and magnetic sand and humus would be almost equally heterogeneous. However, another parameter that quantifies heterogeneity, i.e., variability, is very small in magnetic sand and is moderate in laterite, which makes clutter in these soils relatively small and very large in humus. The discussions lead to the conclusion that there is no simple relationship between the variability and correlation length of soil permittivity distribution and GPR clutter in the case of higher frequency GPR. This is one of the supporting arguments for using the Mie solution for clutter modeling, which fully describes the complicated relationships of these parameters, and not the Rayleigh approximation, which oversimplifies these relationships for relatively high-frequency GPR, although it is still valid for low-frequency GPR.

In this paper, it has also been demonstrated that GPR performance for landmine detection in terms of FAR reduction and POD loss, which were obtained in a field test, was directly related to the amount of GPR clutter caused by soil heterogeneity. The result clearly illustrates that GPR clutter plays a major role in the detection and/or identification of small objects such as antipersonnel landmines buried in heterogeneous soils. The relationship between GPR performance and clutter was demonstrated by modeling GPR clutter based on dielectric permittivity measurements in test soils. Therefore, this modeling can be used for the assessment of GPR performance in a real minefield prior to clearance operations (i.e., in a so-called technical survey) by carrying out rapid TDR measurements, which requires much less time and cost than the actual clearance operations with GPR. By simply calculating expected clutter power for a soil and by comparing to the values of other soils, one can have an idea how difficult the soil is. The method would be even more powerful if it is used as a decision-making tool to judge whether a GPR is usable or not in the analyzed soil by applying a threshold on the calculated clutter power. However, the threshold level may depend on detector models and on the decision made by demining organizations on how much degradation of performance is tolerable. In addition to the evaluation of soil difficulty, the analysis of clutter observed by GPR during the operations can provide confidence levels of survey results. These performance assessment tools can ensure the safety of clearance operations and can help the efficient implementation of GPR (dual-sensor) systems.

ACKNOWLEDGMENT

The authors would like to thank D. Gülle with Mine Action Consulting, and colleagues in the Bundeswehr Technical Centre for Protective and Special Technologies in Oberjettenberg (WTD 52), Germany, for assisting in the geophysical measurements in the field.

REFERENCES

[1] J. MacDonald, J. R. Lockwood, J. McFee, T. Altshuler, T. Broach, L. Carin, R. Harmon, C. Rappaport, W. Scott, and R. Weaver, *Alternatives for Landmine Detection*. Santa Monica, CA, USA: RAND, 2003.

[2] B. Barrow and H. H. Nelson, "Model-based characterization of electromagnetic induction signatures obtained with the MTADS electromagnetic array," *IEEE Trans. Geosci. Remote Sens.*, vol. 39, no. 6, pp. 1279–1285, Jun. 2001.

[3] F. Shubitidze, K. O'Neill, K. Sun, and K. D. Paulsen, "Investigation of broadband electromagnetic induction scattering by highly conductive, permeable, arbitrarily shaped 3-D objects," *IEEE Trans. Geosci. Remote Sens.*, vol. 42, no. 3, pp. 540–556, Mar. 2004.

[4] M.-H. Wei, W. R. Scott, Jr., and J. H. McClellan, "Robust estimation of the discrete spectrum of relaxations for electromagnetic induction responses," *IEEE Trans. Geosci. Remote Sens.*, vol. 48, no. 3, pp. 1169–1179, Mar. 2010.

[5] A. N. Garroway, M. L. Buess, J. B. Miller, B. H. Suits, A. D. Hibbs, G. A. Barrall, R. Matthews, and L. J. Burnett, "Remote sensing by nuclear quadrupole resonance," *IEEE Trans. Geosci. Remote Sens.*, vol. 39, no. 6, pp. 1108–1118, Jun. 2001.

[6] A. Jakobsson, M. Mossberg, M. D. Rowe, and J. A. S. Smith, "Frequency-selective detection of nuclear quadrupole resonance signals," *IEEE Trans. Geosci. Remote Sens.*, vol. 43, no. 11, pp. 2659–2665, Nov. 2005.

[7] S. D. Somasundaram, A. Jakobsson, J. A. S. Smith, and K. Althoefer, "Exploiting spin decay in the detection of nuclear quadrupole resonance signals," *IEEE Trans. Geosci. Remote Sens.*, vol. 45, no. 4, pp. 925–933, Apr. 2007.

[8] C. J. Cumming, C. Aker, M. Fisher, M. Fox, M. J. la Grone, D. Reust, M. G. Rockley, T. M. Swager, E. Towers, and V. Williams, "Using novel fluorescent polymers as sensory materials for above-ground sensing of chemical signature compounds emanating from buried landmines," *IEEE Trans. Geosci. Remote Sens.*, vol. 39, no. 6, pp. 1119–1128, Jun. 2001.

[9] J. M. Sabatier and N. Xiang, "An investigation of acoustic-to-seismic coupling to detect buried antitank landmines," *IEEE Trans. Geosci. Remote Sens.*, vol. 39, no. 6, pp. 1146–1154, Jun. 2001.

[10] W. R. Scott, Jr., J. S. Martin, and G. D. Larson, "Experimental model for a seismic landmine detection system," *IEEE Trans. Geosci. Remote Sens.*, vol. 39, no. 6, pp. 1155–1164, Jun. 2001.

[11] Y. Q. Zeng and Q. H. Liu, "Acoustic detection of buried objects in 3-D fluid saturated porous media: Numerical modeling," *IEEE Trans. Geosci. Remote Sens.*, vol. 39, no. 6, pp. 1165–1173, Jun. 2001.

[12] K. Khanafer, K. Vafai, and B. A. Baertlein, "Effects of thin metal outer case and top air gap on thermal IR images of buried antitank and antipersonnel land mines," *IEEE Trans. Geosci. Remote Sens.*, vol. 41, no. 1, pp. 123–135, Jan. 2003.

[13] A. Muscio and M. A. Corticelli, "Land mine detection by infrared thermography: Reduction of size and duration of the experiments," *IEEE Trans. Geosci. Remote Sens.*, vol. 42, no. 9, pp. 1955–1964, Sep. 2004.

[14] H. Brunzell, "Detection of shallowly buried objects using impulse radar," *IEEE Trans. Geosci. Remote Sens.*, vol. 37, no. 2, pp. 875–886, Mar. 1999.

[15] O. Lopera and N. Milisavljevic, "Prediction of the effects of soil and target properties on the antipersonnel landmine detection performance of ground-penetrating radar: A Colombian case study," *J. Appl. Geophys.*, vol. 63, no. 1, pp. 13–23, Sep. 2007.

[16] T. G. Savelyev, L. van Kampen, H. Sahli, J. Sachs, and M. Sato, "Investigation of time-frequency features for GPR landmine discrimination," *IEEE Trans. Geosci. Remote Sens.*, vol. 45, no. 1, pp. 118–129, Jan. 2007.

[17] K. C. Ho, L. Carin, P. D. Gader, and J. N. Wilson, "An investigation of using the spectral characteristics from ground penetrating radar for landmine/clutter discrimination," *IEEE Trans. Geosci. Remote Sens.*, vol. 46, no. 4, pp. 1177–1191, Apr. 2008.

[18] K. Takahashi and M. Sato, "A hand-held dual-sensor system using impulse GPR for demining," in *Proc. IEEE Int. Conf. Ultra-Wideband*, Hannover, Germany, 2008, pp. 157–160.

[19] D. J. Daniels, *Ground Penetrating Radar*., 2nd ed. London, U.K.: IEE, 2004.

[20] D. J. Daniels, *EM Detection of Concealed Targets*. Hoboken, NJ, USA: Wiley, 2010.

[21] H. M. Jol, *Ground Penetrating Radar: Theory and Applications*. Amsterdam, The Netherlands: Elsevier, 2009.

[22] "Humanitarian mine action—Test and evaluation—Part 1: Metal detectors," Brussels, Belgium, CWA 14747-1, 2003.

[23] K. Takahashi, J. Igel, and H. Preetz, "Influence of soil inhomogeneity on GPR for landmine detection," in *Proc. 13th Int. Conf. GPR*, Lecce, Italy, Jun. 2010, pp. 11–16.

[24] K. Takahashi, J. Igel, and H. Preetz, "Clutter modeling for ground-penetrating radar measurements in heterogeneous soils," *IEEE J. Sel. Topics Appl. Earth Observ.*, vol. 4, no. 4, pp. 739–747, Dec. 2011.

[25] K. Takahashi, J. Igel, and H. Preetz, "Modeling GPR clutter caused by soil heterogeneity," *Int. J. Antennas Propag.*, vol. 2012, pp. 643 430-1–643 430-7, Jan. 2012.

[26] K. Takahashi, J. Igel, and H. Preetz, "Soil properties and performance of landmine detection by metal detector and ground-penetrating radar—Soil

characterisation and its verification by a field test," *J. Appl. Geophys.*, vol. 73, no. 4, pp. 368–377, Apr. 2011.
[27] G. C. Topp, J. L. Davis, and A. P. Annan, "Electromagnetic determination of soil water content: Measurements in coaxial transmission lines," *Water Resourc. Res.*, vol. 16, no. 3, pp. 574–582, Jun. 1980.
[28] L. C. Shen, W. C. Savre, J. M. Price, and K. Athavale, "Dielectric properties of reservoir rocks at ultra-high frequencies," *Geophysics*, vol. 50, no. 4, pp. 692–704, Apr. 1985.
[29] C. V. Deutsch and A. G. Journel, *GSLIB Geostatistical Software Library and User's Guide*. New York, NY, USA: Oxford Univ. Press, 1992.
[30] J. Rea and R. Knight, "Geostatistical analysis of ground-penetrating radar data: A means of describing spatial variation in the subsurface," *Water Resourc. Res.*, vol. 34, no. 3, pp. 329–339, Mar. 1998.
[31] E. H. Issaks and P. M. Srivastava, *An Introduction to Applied Geostatistics*. New York, NY, USA: Oxford Univ. Press, 1989.
[32] P. Goovaerts, *Geostatistics for Natural Resources Evaluation*. New York, NY, USA: Oxford Univ. Press, 1997.
[33] A. B. McBratney and R. Webster, "Choosing functions for semivariograms of soil properties and fitting them to sampling estimates," *J. Soil Sci.*, vol. 37, no. 4, pp. 617–639, Dec. 1986.
[34] A. Ishimaru, *Wave Propagation and Scattering in Random Media*. New York, NY, USA: Academic, 1978.
[35] C. F. Bohren and D. R. Huffman, *Absorption and Scattering of Light by Small Particles*. New York, NY, USA: Wiley, 1983.
[36] H. Preetz, K. Takahashi, and J. Igel, Physical Characterisation of the Test Lanes in the ITEP Dual Sensor Test Oberjettenberg/Germany 2009, Leibniz Inst. for Appl. Geophys., Hanover, Germany, ITEP Project Rep. [Online]. Available: http://www.itep.ws/pdf/OberjettenbergDStest_soilsLIAG2009.pdf
[37] D. K. Butler, *Near-Surface Geophysics*. Tulsa, OK, USA: SEG, 2005.
[38] K. Takahashi and D. Gülle, "ITEP dual sensor test in Germany," in *Proc. 7th Int. Symp. Humanitarian Demining*, Sibenik, Croatia, 2010, pp. 10–14.
[39] K. Takahashi and D. Gülle, "ITEP evaluation of metal detectors and dual-sensor detectors," *J. ERW Mine Action*, vol. 14.3, pp. 76–79, 2010.
[40] B. Lampe, K. Holliger, and A. G. Green, "A finite time-domain simulation tool for ground-penetrating radar antennas," *Geophysics*, vol. 68, no. 3, pp. 971–987, May/Jun. 2003.

Kazunori Takahashi (S'05–M'07) received the A.E. degree in mechanical engineering from Sendai National College of Technology, Sendai, Japan, in 1999, the B.E. degree in mechanical engineering from Yamagata University, Yamagata, Japan, in 2001, and the M.E. and Ph.D. degrees in geoscience engineering from Tohoku University, Sendai, in 2003 and 2006, respectively.

He joined the Center for Northeast Asian Studies, Tohoku University, in 2006 as a Research Associate. He was a Research Scientist with the Federal Institute for Materials Research and Testing (BAM), Berlin, Germany, from 2007 to 2009 and with the Leibniz Institute for Applied Geophysics, Hannover, Germany, from 2009 to 2011, and then, he worked as an Assistant Professor with the Graduate School of Science, Tohoku University. He has been an Assistant Professor with the Center for Northeast Asian Studies, Tohoku University, since 2013. His current research interests include the development of ground-penetrating radar systems and their applications, and analysis methods, inverse problems, landmine detection for humanitarian demining, and nondestructive testing.

Dr. Takahashi was a recipient of the Young Researcher Award of the 13th International Conference on Ground Penetrating Radar in 2010.

Jan Igel received the M.Sc. (diploma) degree in geophysics from Karlsruhe University (TH), Karlsruhe, Germany, in 2001 and the Ph.D. degree in geosciences from Johann Wolfgang Goethe University, Frankfurt, Germany, in 2007.

He joined the Geoelectrics and Electromagnetics Department, Leibniz Institute for Applied Geophysics, Hannover, Germany, in 2001. His current research interests include hydrogeophysics, near-surface investigations, and modeling the influence of soil heterogeneity on geophysical data. He has been working on the problem of soil impact on landmine detection for several years.

Dr. Igel is a member of the European Geosciences Union and the German Geophysical Society (DGG).

Holger Preetz received the degree in physical geography and soil science from the University of Frankfurt, Frankfurt, Germany, and the Ph.D. degree from the University of Halle, Halle, Germany.

He worked for 14 years on soil contamination and remediation and also on the detection of UXO. For the past nine years, he did research on soil influence on landmine detection at the Leibniz Institute for Applied Geophysics, Hannover, Germany. He recently started working at the Department of UXO Clearance, Financial Administration, Hannover.

Motoyuki Sato (S'79–M'80–SM'02–F'10) received the B.E., M.E., and Dr.Eng. degrees in information engineering from Tohoku University, Sendai, Japan, in 1980, 1982, and 1985, respectively.

Since 1997, he has been a Professor with Tohoku University, where he has been a Distinguished Professor since 2007 and where he was the Director of the Center for Northeast Asian Studies in 2009–2013. From 1988 to 1989, he was a Visiting Researcher with the Federal German Institute for Geoscience and Natural Resources (BGR), Hannover, Germany. He is a Visiting Professor with Jilin University, Changchun, China; Delft University of Technology, Delft, The Netherlands; and Mongolian University of Science and Technology, Ulaanbaatar, Mongolia. He has conducted the development of GPR sensors for humanitarian demining, and his sensor ALIS, which is a handheld dual sensor, has detected more than 80 mines in minefields in Cambodia since May 2009. His current interests include transient electromagnetics and antennas, radar polarimetry, ground-penetrating radar (GPR), borehole radar, electromagnetic induction sensing, and interferometric and polarimetric SAR.

Dr. Sato has been a member of the GRSS Administrative Committee since 2006, where he is responsible for specialty symposia and Asian issues. He is an Associate Editor of the IEEE GEOSCIENCE AND REMOTE SENSING LETTERS and a Guest Editor of the special issue of GPR2006 and GPR2010 in the IEEE TRANSACTIONS ON GEOSCIENCE AND REMOTE SENSING and IGARSS2011 and GPR2012 in the IEEE JOURNAL OF SELECTED TOPICS IN APPLIED EARTH OBSERVATIONS AND REMOTE SENSING. He was the Chair of the IEEE GRSS Japan Chapter in 2006–2007. He served as the General Chair of IGARSS2011.